Molecular Therapy
Methods & Clinical Development
Original Article

AAV-mediated *PEX1* gene augmentation improves visual function in the PEX1-Gly844Asp mouse model for mild Zellweger spectrum disorder

Catherine Argyriou,[1,4] Anna Polosa,[2,4] Ji Yun Song,[3] Samy Omri,[4] Bradford Steele,[5] Bruno Cécyre,[6] Devin S. McDougald,[3] Erminia Di Pietro,[4] Jean-François Bouchard,[6] Jean Bennett,[3] Joseph G. Hacia,[5] Pierre Lachapelle,[2,4] and Nancy E. Braverman[1,4]

[1]Department of Human Genetics, McGill University, Montreal, QC, Canada; [2]Department of Ophthalmology & Visual Sciences, McGill University, Montreal, QC, Canada; [3]Center for Advanced Retinal and Ocular Therapeutics, F.M. Kirby Center for Molecular Ophthalmology, Perelman School of Medicine, University of Pennsylvania, Philadelphia, PA, USA; [4]Research Institute of the McGill University Health Centre, Montreal, QC, Canada; [5]Department of Biochemistry and Molecular Medicine, Keck School of Medicine, University of Southern California, Los Angeles, CA, USA; [6]School of Optometry, Université de Montréal, Montreal, QC, Canada

Patients with Zellweger spectrum disorder (ZSD) commonly present with vision loss due to mutations in *PEX* genes required for peroxisome assembly and function. Here, we evaluate *PEX1* retinal gene augmentation therapy in a mouse model of mild ZSD bearing the murine equivalent (PEX1-p[Gly844Asp]) of the most common human mutation. Experimental adeno-associated virus 8.cytomegalovirus.human PEX1.hemagglutinin (AAV8.CMV.*HsPEX1.HA*) and control AAV8.CMV.*EGFP* vectors were administered by subretinal injection in contralateral eyes of early (5-week-old)- or later (9-week-old)-stage retinopathy cohorts. HsPEX1.HA protein was expressed in the retina with no gross histologic side effects. Peroxisomal metabolic functions, assessed by retinal C26:0 lysophosphatidylcholine (lyso-PC) levels, were partially normalized after therapeutic vector treatment. Full-field flash electroretinogram (ffERG) analyses at 8 weeks post-injection showed a 2-fold improved retinal response in the therapeutic relative to control vector-injected eyes. ffERG improved by 1.6- to 2.5-fold in the therapeutic vector-injected eyes when each cohort reached 25 weeks of age. At 32 weeks of age, the average ffERG response was double in the therapeutic relative to control vector-injected eyes in both cohorts. Optomotor reflex analyses trended toward improvement. These proof-of-concept studies represent the first application of gene augmentation therapy to treat peroxisome biogenesis disorders and support the potential for retinal gene delivery to improve vision in these patients.

INTRODUCTION

Zellweger spectrum disorders (ZSDs) are autosomal-recessive disorders typically caused by biallelic mutations in any of 13 *PEX* genes, which encode PEX proteins or peroxins, required for peroxisome assembly and functions. Peroxisomes are subcellular organelles with vital roles in lipid metabolism.[1–4] Deleterious variants in *PEX1* account for about 70% of ZSD cases in North America, with the hypomorphic *PEX1*-c.[2528G > A] allele representing about 30% of these variants.[2,3,5,6] The latter encodes the partially functional PEX1-p.[Gly843Asp] protein (PEX1-G843D), which is capable of supporting residual peroxisome assembly and function. Due to this residual function, the PEX1-p.[Gly843Asp] allele is associated with milder clinical pictures typically characterized by degenerative phenotypes without major congenital defects.[7–9]

PEX1 and its binding partner PEX6 are AAA ATPases (ATPases associated with various cellular activities) that form the peroxisome "exportomer" complexes, anchored to the peroxisome membrane by PEX26.[10] After PEX5 shuttles nascent peroxisomal enzymes to the peroxisome membrane for matrix import, the exportomer complex recycles PEX5 from the peroxisome membrane to the cytoplasm for additional rounds of enzyme import.[11–13] If not recycled, PEX5 is targeted for proteasomal degradation, peroxisome matrix protein import is impaired, and metabolic dysfunction ensues.[14] Hallmark clinical biomarkers of peroxisome dysfunction in ZSD include the accumulation of potentially toxic very long chain and branched chain fatty acids, and diminished plasmalogens, important membrane ether phospholipids.[15]

In addition to variable multisystem presentations,[1,16] most ZSD patients develop progressive vision loss, primarily (but not always exclusively) due to retinal abnormalities, particularly photoreceptor loss.[17,18] Although milder ZSD patients are typically born with functional vision, they often develop retinitis pigmentosa, macular atrophy, reduced visual acuity, and reduced or extinguished electroretinograms (ERGs).[19–21] Other less common ocular manifestations include retinal arteriolar attenuation, optic nerve atrophy, nystagmus, and foveal thinning.[17,19,22] Given their progressive vision loss,

Received 10 March 2021; accepted 1 September 2021;
https://doi.org/10.1016/j.omtm.2021.09.002.

Correspondence: Catherine Argyriou, Research Institute of the McGill University Health Centre, 1001 Decarie Blvd., EM0.2248, Montreal, QC H4A 3J1, Canada.
E-mail: catherine.argyriou@mail.mcgill.ca

interventions that rescue peroxisome function at an early stage could slow or prevent retinal deterioration, which would have a major impact on communication, learning, mobility, autonomy, and overall life quality.

To assess whether various experimental therapies could slow the loss of or improve retinal functions in people with milder ZSD, we characterized visual functions in the homozygous PEX1-G844D mouse model of milder ZSD, which harbors the murine equivalent of the common human PEX1 (HsPEX1)-G843D allele.[23] This model exhibits diminished cone photoreceptor function to 32 weeks, with rod photoreceptor function diminishing over time, and reduced visual acuity.[24] PEX1-G844D mice also exhibit decreased cone cell numbers through life, decreased bipolar cell numbers with age, and photoreceptor inner-segment disorganization.[24] Since these phenotypes strongly reflect the degenerative retinal disease found in milder patients, this milder ZSD mouse model provides a robust platform for interventional testing.

Given the successes of recombinant adeno-associated virus (rAAV)-mediated retinal gene augmentation therapy for monogenic ocular diseases,[25–27] we evaluated the ability of retinal AAV-mediated *PEX1* gene augmentation therapy to slow or prevent vision loss in the homozygous PEX1-G844D mouse model. After confirming that *HsPEX1* expression recovered peroxisome functions in murine and human *PEX1*-deficient cells, we evaluated the effects of AAV8.cytomegalovirus (CMV).*HsPEX1*.hemagglutinin (*HA*) delivered by subretinal injection into the eyes of 5- and 9-week-old homozygous PEX1-G844D mice. Our outcome measures included HsPEX1 protein expression, effect on retinal function, and visual acuity over the course of 6–7 months. Overall, the data we collected represent the first testing of gene therapy to treat a peroxisome biogenesis disorder, demonstrate therapeutic windows for addressing retinal degeneration in this mouse model, and provide proof-of-concept evidence for the potential of gene augmentation approaches to address the degenerative aspects of milder ZSD.

RESULTS

Recovery of peroxisome import by HsPEX1 delivery in human and mouse cells

The CMV.*HsPEX1.HA* expression cassette used in these studies consisted of codon-optimized *HsPEX1* (sequence in Supplemental materials and methods) with a C-terminal HA epitope tag (Figure 1A) or EGFP (Figure 1B) transgenes, driven by a CMV enhancer/promoter and terminating into a bovine growth hormone (bGH) polyadenylation signal. This expression cassette was flanked by canonical AAV2-inverted terminal repeats (ITRs) and packaged into the AAV8 capsid. We included the HA tag to distinguish vector-delivered protein from the endogenous mouse PEX1-G844D. This AAV8.CMV.*HsPEX1.HA* vector was tested for expression of full-length PEX1 protein using HEK293 84-31 cells transduced with AAV8.CMV.*HsPEX1.HA* or AAV8.CMV.EGFP at a multiplicity of infection (MOI) of 10^5 or 5×10^5 vector genomes (vgs) per cell. Immunoblotting against the HA tag revealed a single band corresponding to the size of PEX1, with greater intensity at the higher compared to lower MOI (Figure 1C). As expected, no HA tag was detected in cells transduced with AAV8.CMV.*EGFP*, which showed a band corresponding to the size of GFP when probed with anti-GFP antibody.

To ensure that the HA tag does not interfere with PEX1 function, we evaluated peroxisome recovery using a *PEX1* null HepG2 cell line generated by CRISPR-Cas9 genome editing (Figure S1A and Supplemental materials and methods). We used this cell type as it was more efficiently transduced by AAV8 than patient fibroblasts.[28] *PEX1* null HepG2 cells were transduced at an MOI of 10^5 with AAV8.CMV.*HsPEX1.HA* and visualized after 48 h by immunofluorescent (IF) microscopy. In control cells, enzymes with the C-terminal peroxisome targeting signal 1 (PTS1) motif are localized to peroxisomes, co-localizing with the peroxisome membrane protein ATP Binding Cassette Subfamily D Member 3 (ABCD3). In cells with a *PEX1* defect, PTS1-containing proteins are not imported by peroxisomes and thus localized to the cytosol and reportedly degraded.[29] AAV8-mediated expression of HA-tagged PEX1 recovered PTS1 protein localization in PEX1 null HepG2 cells (Figure 1D), indicating that the tagged transgene is functional. Viral transduction did not impact PTS1 protein localization in control HepG2 cells (Figure S1B).

Overall, HsPEX1 and mouse PEX1 proteins share 82% identity.[23] To confirm that HsPEX1 is functional within the mouse exportomer complex, primary mouse fibroblasts homozygous for PEX1-G844D were engineered to express HsPEX1. As AAV8 does not efficiently transduce fibroblasts, a modified lentiviral vector was used to deliver *HsPEX1* (GenBank: NM_000466.2; see Materials and methods). As a negative control, we used the same vector backbone modified to express *HsPEX1*-c.2097_2098insT, encoding a common *PEX1* null allele.[30] IF microscopy was performed on wild-type and PEX1-G844D primary murine fibroblasts stably expressing each transgene. In wild-type cells, PTS1-containing proteins were punctate and co-localized with ABCD3 under all conditions. In PEX1-G844D cells, PTS1 proteins were primarily cytosolic at baseline but redistributed to punctate localization exclusively following *HsPEX1* delivery, indicating recovered peroxisome import (Figures 2A and S2A). As a complimentary measure, localization of the PEX5 peroxisome shuttle protein was visualized. In wild-type cells, PEX5 is primarily cytosolic and remains so regardless of intervention (Figures 2B and S2B). In PEX1-G844D cells, PEX5 appears punctate and co-localizes with ABCD3, indicating it is trapped at the peroxisome membrane. Localization is recovered to the cytosol following HsPEX1 expression, indicating that HsPEX1 functions to remove murine PEX5 from the peroxisome membrane for additional rounds of import.

AAV8-mediated HsPEX1.HA protein is expressed in mouse retina, and visual function improves by 8 weeks post-subretinal gene delivery

The effect of AAV8-mediated gene delivery was tested at 2 different ages: mice injected at (1) 5 weeks of age, representing a "prevention" cohort, when the scotopic full-field flash ERG (ffERG) response is highest in the PEX1-G844D model, or (2) 9 weeks of age, representing a "recovery" cohort, when the ffERG response has begun declining.[24]

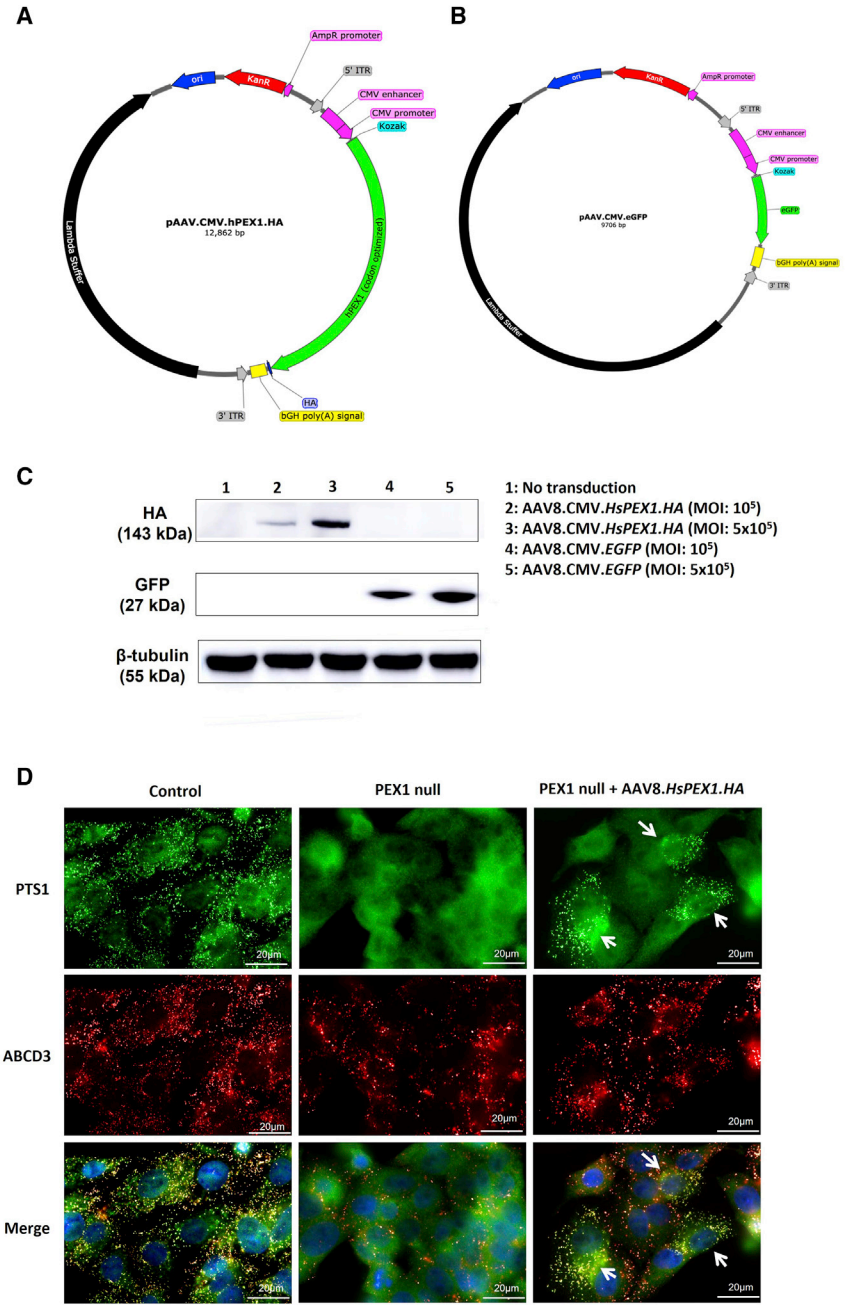

Figure 1. Proviral plasmid design and rAAV8 human *PEX1* (*HsPEX1*) vector expression

Constructs were designed to deliver (A) codon-optimized *HsPEX1* cDNA with a C-terminal HA epitope tag and (B) *EGFP* cDNA. Both are driven by a CMV enhancer/promoter and terminate with a bovine growth hormone (bGH) polyadenylation signal. The expression cassette is flanked by the canonical AAV2 inverted terminal repeats (ITRs) and was packaged into an AAV8 vector. (C) Expression of AAV8-delivered proteins in HEK293 84-31 cells: after transduction with AAV8.CMV.*HsPEX1.HA*, immunoblotting of cell lysates showed a single 143-kDa band, corresponding to the size of PEX1, after probing the membrane with anti-HA antibody. Probing with anti-GFP antibody yielded single bands at 27 kDa in cells transduced with AAV8.CMV.*EGFP*, matching the size of GFP. β-tubulin (55 kDa) was used as a loading control. (D) Expression of HsPEX1 in HepG2 cells: control cells exhibit punctate peroxisome targeting signal 1 (PTS1)-containing protein distribution that co-localizes with the peroxisome membrane protein ABCD3. In contrast, PTS1 is cytoplasmic in PEX1 null cells (see also Figure S1A). After transduction with AAV8.CMV.*HsPEX1*.HA, PTS1 redistributes from the cytosol to peroxisomes (puncta, white arrows), indicating recovered peroxisome import. As the AAV-delivered transgene cassette is episomal and thus diluted with each cell division, only a few rescued cells are seen per field of view. Images were visualized by indirect immunofluorescent (IF) microscopy at 60× magnification with PTS1 (green) and peroxisome membrane protein ABCD3 (red), colocalization (yellow), and DAPI nuclear staining (blue). There was no fluorescent signal when no primary antibody was applied, and transduction did not alter PTS1 localization in HepG2 control cells (see Figure S1B).

G844D and wild-type littermate mice received 10^{10} vg AAV8.CMV.*HsPEX1.HA* in the left eye and AAV8.CMV.*EGFP* in the right eye by subretinal injection. A smaller "validation" cohort was established to confirm vector expression *in vivo* and have an earlier review of experimental results. "Non-injected" mutants and wild-type littermates were included in each cohort, received no intervention, and served as controls for the surgical procedure. Figure 3 is a schematic representation of the experimental design.

For the prevention cohort, we selected to treat at 5 weeks of age to allow for obtaining baseline ffERGs at maximal rod response and to see if treatment would prevent the functional decline observed in untreated mutants. ffERGs were recorded for all mice in the week prior to injection (waveforms and quantification are shown in Figure S3). Although our model exhibits a large variation in the ffERG response, there was no difference between the average left versus right eye values. To account for this phenotypic variation, we used the contralateral eye of each treated animal as a control: homozygous PEX1-

In the validation cohort, 4 mice were sacrificed 4 weeks post-injection to confirm HsPEX1.HA protein expression. Immunohistochemistry (IHC) against the HA tag on retinal flatmounts showed spots of concentrated expression in the retinal pigment epithelium (RPE) (Figure 4A) and more widespread expression of varying level throughout the photoreceptor side of the neural retina (Figure 4B). Retinal immunoblotting showed PEX1 protein levels markedly increased over baseline in the *HsPEX1*-injected tissues (Figure 4C).

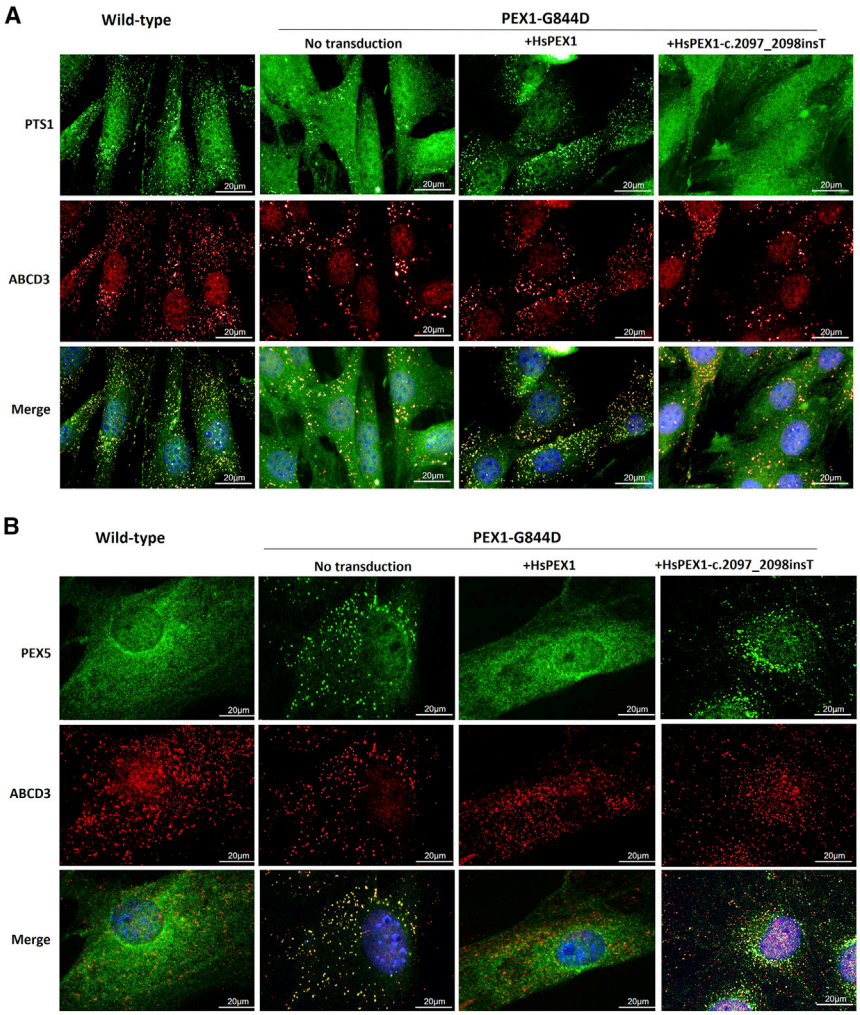

Figure 2. HsPEX1 recovers peroxisome import and PEX5 localization in murine PEX1-G844D primary fibroblasts after lentiviral transduction

(A) In control mouse cells, PTS1-containing proteins exhibited punctate distribution that co-localized with the peroxisome membrane protein ABCD3. Homozygous PEX1-G844D mouse cells exhibited more cytosolic PTS1 protein localization with partial import. Expression of *HsPEX1* resulted in complete recovery of PTS1 protein localization to peroxisomes, whereas transduction with non-functional *HsPEX1* (*HsPEX1*-c.2097_2098insT, which encodes a null mutation) did not recover import. (B) In control mouse cells, the peroxisomal receptor PEX5 was distributed throughout the cytosol. In homozygous PEX1-G844D mouse cells, PEX5 was primarily localized at peroxisomes. Expression of wild-type *HsPEX1* resulted in relocalization of murine PEX5 to the cytosol, indicating recovered PEX5 recycling, whereas expression of non-functional *HsPEX1* (*HsPEX1*-c.2097_2098insT, which encodes a null mutation) did not recover PEX5 cytosolic location. Images were visualized by indirect IF microscopy at 60× magnification with PTS1 or PEX5 (green) and peroxisome membrane protein ABCD3 (red), colocalization (yellow), and DAPI nuclear staining (blue). There was no fluorescent signal when no primary antibody was applied, and AAV8 transduction did not affect peroxisome import or PEX5 localization in wild-type cells (see Figure S2).

ffERGs were performed 8 weeks following gene delivery on the remaining 8 PEX1-G844D mice in the cohort and 8 non-injected mutant controls. There was no difference in average rod-mediated (scotopic) a-wave values among treatment groups; although the average scotopic b-wave trended toward improvement, it did not meet statistical significance (Figure 5A). However, the average cone-mediated (photopic) ffERG response of the *HsPEX1*-injected (left) eyes was two-fold that of the *EGFP*-injected (right) eyes (32 μV versus 17 μV, respectively, $p = 0.048$) and more than 2-fold that of the non-injected left or right eyes (10 μV and 13 μV, respectively, $p = 0.0015$ and $p = 0.015$). Visual acuity was determined using the OptoMotry system (see Materials and methods) to measure the optomotor reflex (OMR) 11 weeks after subretinal gene delivery when this cohort was 16 or 20 weeks old. Although the average visual acuity was nearly 4-fold higher in the left versus right eyes (0.130 versus 0.034 cycle/degree, c/d), this difference was narrowly below statistical significance ($p = 0.054$) (Figure 5B).

This remaining validation cohort was sacrificed 12 weeks after subretinal injection to confirm HsPEX1-HA or EGFP expression in retinal sections. The HA tag was mainly localized to the photoreceptor inner segment and the outer plexiform layer (Figure 5C, left panel), matching the reported sites of endogenous murine PEX1 enrichment,[24,31,32] suggesting that the vector-delivered gene is translated and appropriately localized. EGFP expression was more diffuse, extending from the RPE to the outer plexiform layer (Figure 5C, right panel). IHC was performed across all retinal sections from each eye, and all sections from each retina were qualitatively scored for intensity of protein expression and degree of coverage. Although all 8 retinas were positive for HA-tag or EGFP expression, the location, scope, and amount of expression were variable, as seen in the representative "high," "medium," and "low" expression intensities shown in Figure 5. Expression was strongest at the injection site (located toward the nasal end of the eye) and gradually diminished with distance (Figure 5D). Approximately 30% of the outer retina in each mouse was positive for some degree of expression. There was no apparent effect on gross retinal histology after subretinal injection nor HA localization within the nuclear layers.

Retinal function but not functional vision improves 6 or 7 months post-subretinal gene delivery

In the recovery and prevention cohorts, ffERGs were recorded on a subset of animals (6) when each cohort reached 25 weeks of age (16

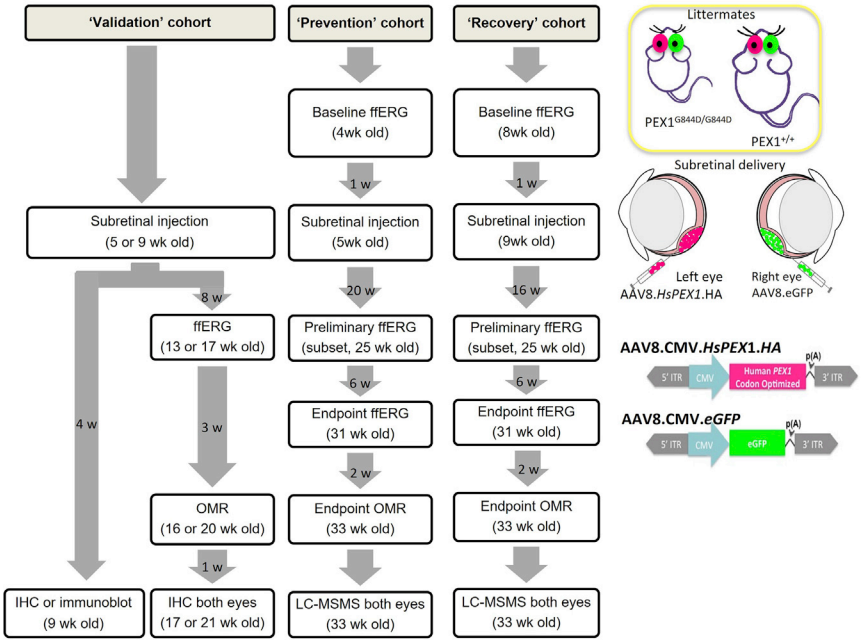

Figure 3. Diagram of experimental design of preclinical trial

The effect of AAV8-mediated gene delivery was tested by full-field flash electroretinogram (ffERG) and visual acuity (optomotor reflex [OMR]) at two different ages, representing "prevention" and "recovery" cohorts, exposed to vector for 7 or 6 months, respectively. A "validation" cohort was used to obtain preliminary functional measures and validate vector expression in retina. Homozygous PEX1-G844D and wild-type littermate mice received AAV8.CMV.*HsPEX1.HA* (left eye) and AAV8.CMV.EGFP (right eye) by subretinal injection. Non-injected PEX1-G844D and wild-type mice were included in each cohort. The flow chart shows the ages of mice at intervention and assessment and time between each event. Both eyes were analyzed at experimental endpoint for each cohort.

or 20 weeks after gene delivery, respectively). In the prevention cohort, the average scotopic a-wave was 1.6-fold higher in the left- versus right-injected eyes (87 μV versus 53 μV, p = 0.024), the scotopic b-wave 1.7-fold higher (308 μV versus 176 μV, p = 0.004), and the photopic b-wave 2.7-fold improved (49 μV versus 18 μV, p = 0.002) (Figure 6A). In the recovery cohort, the average scotopic b-wave response was 2.7-fold higher in the left versus right eye (106 μV versus 42 μV, p = 0.035) (Figure 6B). Although the average scotopic a-wave response was 1.6-fold higher in the left versus right eyes of the recovery cohort (60 μV versus 38 μV) and the photopic b-wave 2.5-fold higher (20 μV versus 8 μV), this effect was not statistically significant.

Endpoint ffERGs were performed when each cohort reached 31 weeks of age, 6 or 7 months post-gene delivery for the recovery or prevention cohorts, respectively. In both cohorts, the average scotopic a-wave, scotopic b-wave, and photopic b-wave amplitude of the therapeutic vector-treated (left) eyes was 2-fold that of the control-injected (right) eyes (Figures 7A and 7B). In homozygous PEX1-G844D mice, the retinal response of the control-injected (right) eyes did not differ from that of either eye in non-injected mutant concurrent controls (Figures 7A and 7B). All ffERG endpoint waveforms are shown in Figure S4.

OMR measures were acquired at the experimental endpoint. For both cohorts, average visual acuity trended higher in the *HsPEX1*-injected (left) versus GFP-injected (right) eyes (0.133 c/d versus 0.100 c/d for prevention, 0.120 c/d versus 0.101 c/d for recovery, respectively), but this was not statistically significant (p = 0.381 and p = 0.394, respectively) (Figures 7A and 7B). For both ffERG and visual acuity measures, there was no difference between wild-type mice with or without subretinal injection. Thus, these values are grouped together in Figures 6 and 7.

Subretinal gene delivery slows the decline in rod function and improves cone function

PEX1-G844D mice exhibit a gradual decline in rod-mediated ffERG response (scotopic a- and b-wave amplitudes).[24] Overall, this was ameliorated in *HsPEX1*-injected eyes compared to non-injected eyes when comparing baseline to endpoint ffERGs in both cohorts (Figures 8A and 8B). This trend reached statistical significance in the recovery scotopic b-wave measures (47% versus 84% decline, p = 0.048). More prominently, the endpoint photopic ffERG response in *HsPEX1*-injected eyes improved 242% over baseline compared to 68% in non-injected eyes in the prevention cohort (p = 0.045) and 82% versus −33% in the recovery cohort (p = 0.035). A limitation of this comparison is that baseline ffERGs were not acquired in contralateral control (right) eyes prior to injection with AAV8.CMV.*EGFP*.

Retinal peroxisome metabolites partially normalize following subretinal HsPEX1 gene delivery

In general, impaired peroxisomal metabolism results in increased C26:0 very long chain fatty acids (VLCFAs) and decreased plasmalogens.[33] VLCFA (C26:0 lysophosphatidylcholine [lyso-PC]) and phosphoethanolamine (PE) plasmalogen levels were measured by liquid chromatography-tandem mass spectrometry (LC-MS/MS) in mouse retinas at experimental endpoints (Figure 9A). Average C26:0 lyso-PC levels in the untreated mutants were increased 5- to 7-fold compared to wild-type in the prevention and recovery cohorts. In the prevention cohort only, these values were lowered by 70% compared to contralateral *EGFP*-injected eyes following *HsPEX1* gene augmentation (2-fold versus 7-fold average elevation, p = 0.013), eliminating any significant difference from wild type. This downstream normalization in C26:0 lyso-PC provides direct evidence for improvement of retinal peroxisome functions, at least in the earlier-treated cohort. As previously reported, total PE plasmalogen levels were unaffected in mutant retinas,[24] and this was not altered by gene delivery (Figure 9B).

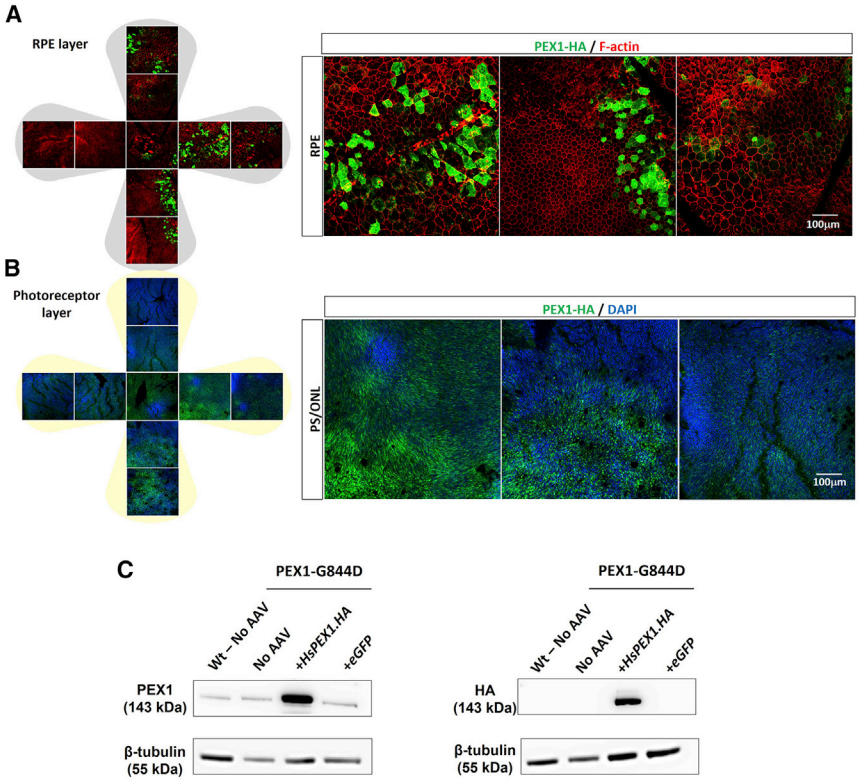

Figure 4. Validation cohort: *in vivo* confirmation of HsPEX1.HA expression

Retinas from PEX1-G844D mice were examined 4 weeks following subretinal injection of AAV8.CMV.*HsPEX1.HA*. 9 different retinal flatmount regions were visualized by confocal microscopy. (A) In the RPE, the HA tag (green) was highly expressed in discrete locations; F-actin of RPE cells was counterstained with rhodamine phalloidin (red). (B) In the neural retina (photoreceptor side), the HA tag (green) showed broader expression of varying intensity; nuclei were counterstained with DAPI. Right panels show higher magnification corresponding to regions of high, medium, and low HA expression. (C) Immunoblotting of retinal lysates showed markedly increased PEX1 in retinas transduced with AAV8.CMV.*HsPEX1.HA* compared to uninjected or AAV8.CMV.*EGFP*-injected samples (left). When the same lysates were probed with anti-HA antibody (right), only the *HsPEX1*-injected retinas yielded a band (corresponding to the size of PEX1). 2 retinas were pooled per sample and 20 μg of protein loaded; β-tubulin was used as a loading control.

DISCUSSION

Almost all patients with ZSD show a progressive loss of vision due to retinal degeneration over time, leading to blindness in childhood or adulthood, depending on disease severity. In its mildest form, ZSD can manifest exclusively as progressive vision and hearing loss with normal cognition due to a variety of *PEX1* and *PEX6* hypomorphic alleles, including PEX1-G843D.[21,22,32,34,35] Although the majority of ZSD patients with an intermediate to milder course have a degenerative disease that affects several organ systems, most notably visual, auditory, nervous, and gastrointestinal systems, there can be long survival, and the visual deficit presents high morbidity. The recent implementation of newborn screening for ZSD and other peroxisomal disorders across the United States[36] provides an unprecedented opportunity to identify individuals with ZSD at the earliest stages of retinal degeneration that represents an optimal therapeutic window for targeted interventions.

Here, we evaluated the potential for retinal gene augmentation therapy in our homozygous PEX1-G844D mouse model. This model exhibits multisystemic involvement, and its other primary phenotypes include growth retardation and fatty liver disease with histological evidence of a bile acid defect associated with intestinal fat malabsorption and cholestasis.[23,37,38] Animals that survive past weaning have a normal lifespan and no overt CNS manifestations. Most importantly, they display degenerative retinal phenotypes corresponding to those found in patients with milder ZSD and thus are a robust model for evaluating targeted therapeutic interventions to slow or prevent vision loss in this patient population.[18,24]

Functional relevance

PEX1-G844D mice typically exhibit a gradual decline in scotopic ffERG and a photopic ffERG that remains consistently diminished from 4 to 32 weeks.[24] Herein, *HsPEX1* gene augmentation resulted in lower scotopic ffERG decline compared to non-injected mutants and improved the photopic response over time in the majority of treated animals. This highlights the potential to slow or prevent the deterioration of retinal response or in the case of photopic ffERG, even improve response. The effect of retinal gene augmentation was relatively greater in the cone- versus rod-mediated response, despite cone function showing earlier degenerative phenotypes in PEX1-G844D mice. There are several possible explanations for this observation. For example, functional improvement in cone cells could be easier to detect, since cone function remains consistently low throughout life in this model, whereas the relative preservation of rod function, and variability therein combined with gradual decline, could partially mask the effect of therapy. Alternatively, it is possible that peroxisome dysfunction affects rods and cones differently and that a small improvement in peroxisome function or an improvement in fewer peroxisome-mediated pathways is sufficient to greatly recover cone function. Finally, AAV8 targeting efficiency for murine rod versus cone photoreceptors may differ, as shown in nonhuman primate studies comparing various AAV serotypes,[39] although we did not observe any differences using the employed techniques.

Based on our studies, the effects of AAV8.CMV.*HsPEX1.HA* delivery are durable to at least 6–7 months (our experimental endpoint),

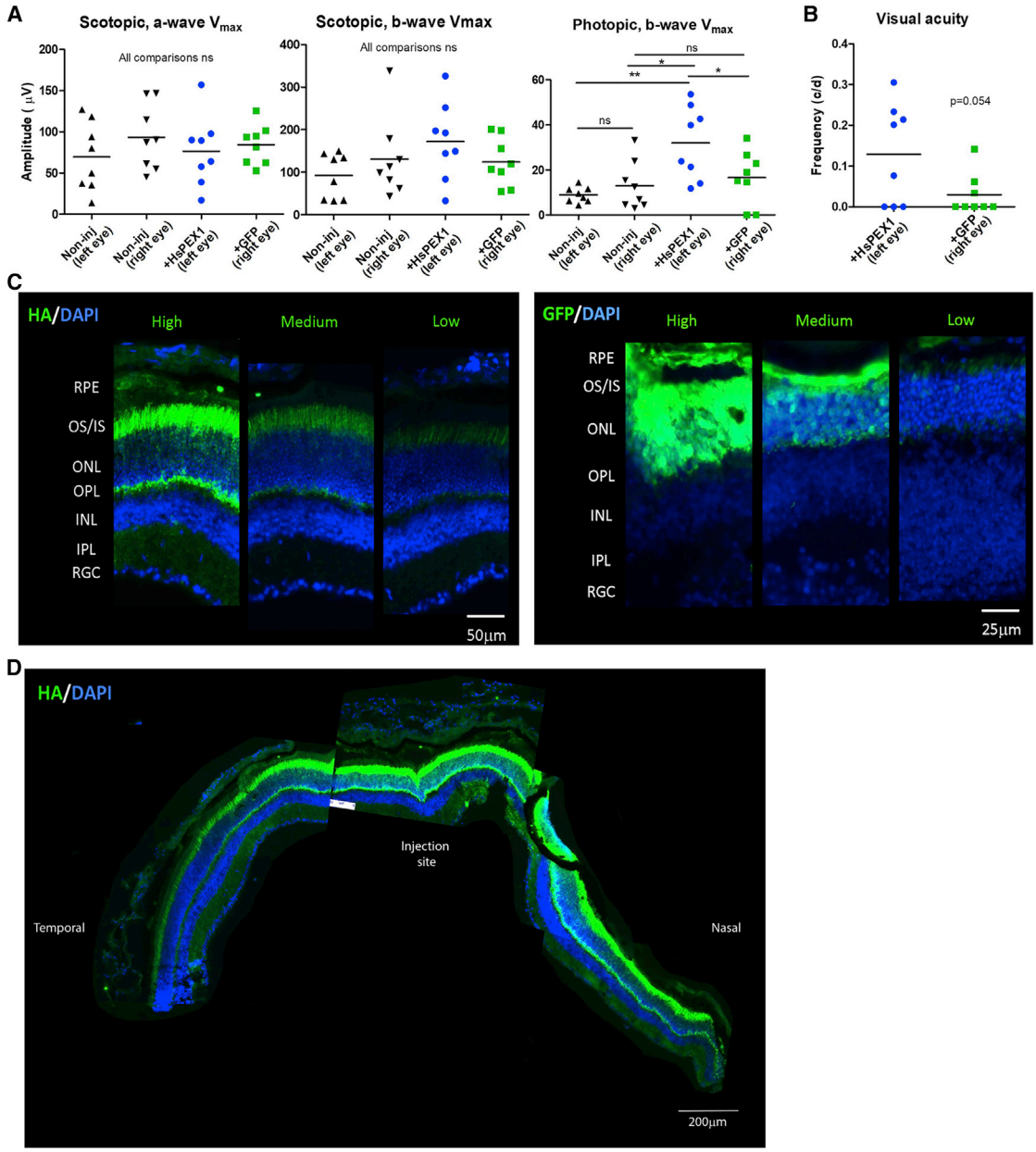

Figure 5. Validation cohort: ffERG, visual acuity, and assessment of rAAV-delivered transgene expression

(A) Quantification of maximum ffERG response 8 weeks post-subretinal injection showed improved average photopic b-wave response in the *HsPEX1*-injected left eye compared to the EGFP-injected right eye or either eye in non-injected controls. The scotopic ffERG response was not significantly altered. The scotopic ffERG response at the highest stimulus interval (0.9 log cd.s.m^{-2}) is shown. (B) Optokinetic analyses 11 weeks post-injection showed a trend toward improved average visual acuity in the *HsPEX1*-injected left eyes compared to right eyes. Mice were tested twice and an average value plotted for each individual eye. Each point represents 1 mouse; Student's t test, *$p < 0.05$, **$p < 0.01$, ***$p < 0.001$, and ns, non-significant at $p < 0.05$. (C) Examination of retinal cryosections by immunohistochemistry showed HsPEX1.HA-tag expression localized to the base of the outer segment/inner segment (OS/IS) interface and outer plexiform layer (OPL), sites of endogenous PEX1 expression, whereas GFP expression was more general, extending to the inner nuclear layer. (D) Expression of HsPEX1.HA-tag expression was strongest at the injection site and toward the nasal end of the eye and gradually diminished with distance. Representative retinal images are shown.

evidenced by functional and biochemical outcome measures. In the PEX1-G844D mouse model, rod-mediated ffERG (scotopic, b-wave) diminishes to below 15% of wild type, on average, by 32 weeks.[24] As variation among mutants also diminishes by this age, we selected this age as the endpoint of our experiments and thus do not know the therapeutic efficacy beyond this point.

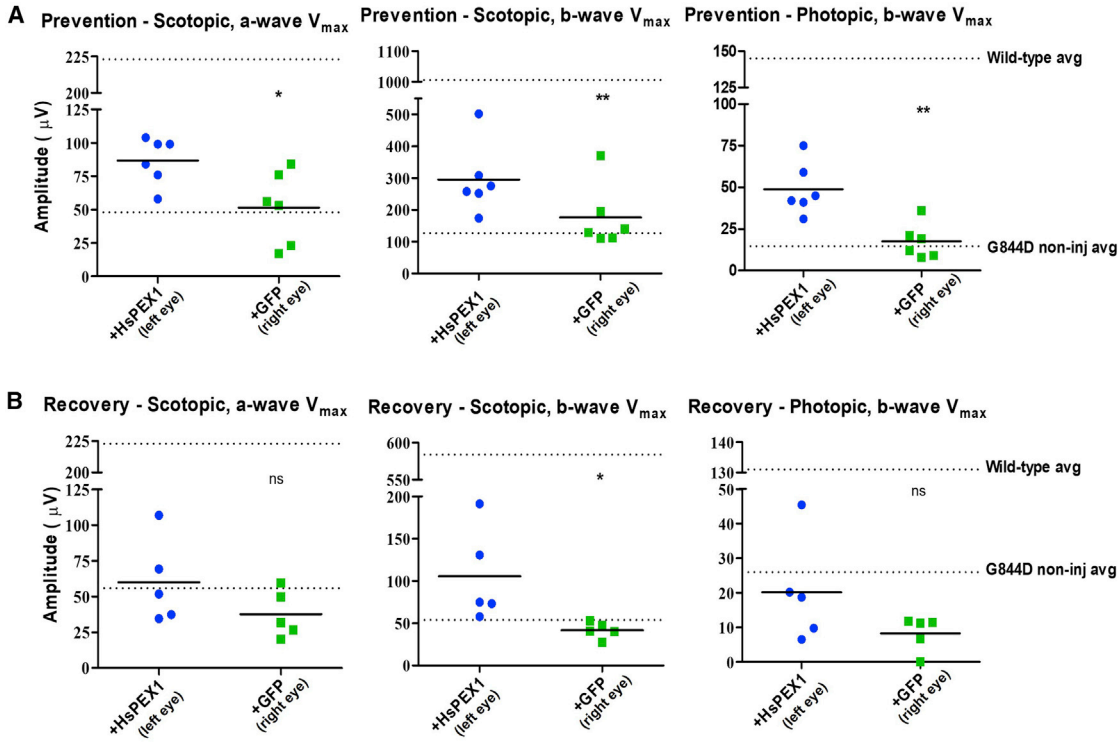

Figure 6. Prevention and recovery cohorts: preliminary ffERG at age 25 weeks (16 or 20 weeks after gene delivery for recovery or prevention cohorts, respectively)

(A) In the prevention cohort, maximal scotopic a-wave, b-wave, and photopic b-wave were improved on average in the *HsPEX1*-injected left- versus *EGFP*-injected right-injected eyes. (B) In the recovery cohort, the average scotopic b-wave response was significantly higher in the left versus right eyes. Scotopic a-wave and photopic b-wave responses trended toward improvement, although not statistically significant. Upper dotted line represents wild-type average and lower dotted line non-injected mutant average (n = 5). Scotopic ffERG response at highest stimulus interval (0.9 log cd.s.m^{-2}) is shown. Each point represents 1 mouse; Student's t test, *p < 0.05, **p < 0.01, ***p < 0.001, and ns, non-significant at p < 0.05.

Despite the 2-fold improvement in scotopic ffERG response over controls 6−7 months post-*HsPEX1* gene augmentation, the scotopic and photopic retinal function of treated mutant mice remained 22%–33% of the wild-type average. As with many therapies in development, a challenge of retinal gene augmentation is determining the sufficient expression level and retinal coverage to meaningfully impact functional vision. In the subset of animals tested 11 weeks following gene delivery, the average visual acuity of therapeutic vector-treated eyes was 4-fold that of the contralateral eyes, and this difference neared statistical significance (p = 0.054). By 6−7 months following gene delivery, only a subtle trend of improved visual acuity compared to the AAV8.CMV.*EGFP*-injected contralateral eyes appeared. Possible reasons for this include the inherent variability in behavioral tests and limitations of performing a single test per mouse, or that not enough cells or correct cell types at any point along the visual pathway (from retina to visual cortex) were rescued to impact functional vision. Considering that full contrast OMR testing in ambient light might mask more subtle but significant functional vision responses, testing could be performed in scotopic conditions, and measures of contrast sensitivity[40] and color perception[41] could be included in future experiments. Of additional note is that transgene expression varied among mice, which may also contribute to outcome variation. In this regard, vector dose escalation experiments could help optimize the scope and degree of therapeutic protein expression, which may improve outcomes.

The progressive retinopathy in PEX1-G844D mice occurs predominantly at the photoreceptor level, with bipolar cells diminishing later in life.[24] Here, we have focused on targeting photoreceptor cells, a known site of endogenous PEX1 enrichment,[24,31,32] using AAV8, which transduces photoreceptors more efficiently than other serotypes.[42] Nevertheless, peroxisomal requirements may be distinct at different retinal layers,[43] and it is unknown if outer retina preservation is sufficient to prevent degeneration at the inner retina. Following subretinal delivery, our vector-delivered proteins are most strongly localized in the photoreceptor outer and inner segment but also consistently expressed up to the outer plexiform layer, the site of photoreceptor and bipolar cell synapses, as well as in the RPE. Expanded RPE analyses should be considered for subsequent studies, as RPE involvement has been recently implicated in a mouse model for peroxisomal multifunctional protein 2 deficiency (MFP2D), which lacks the central enzyme of the peroxisomal β-oxidation pathway.[44] Although recent data in our model suggest that

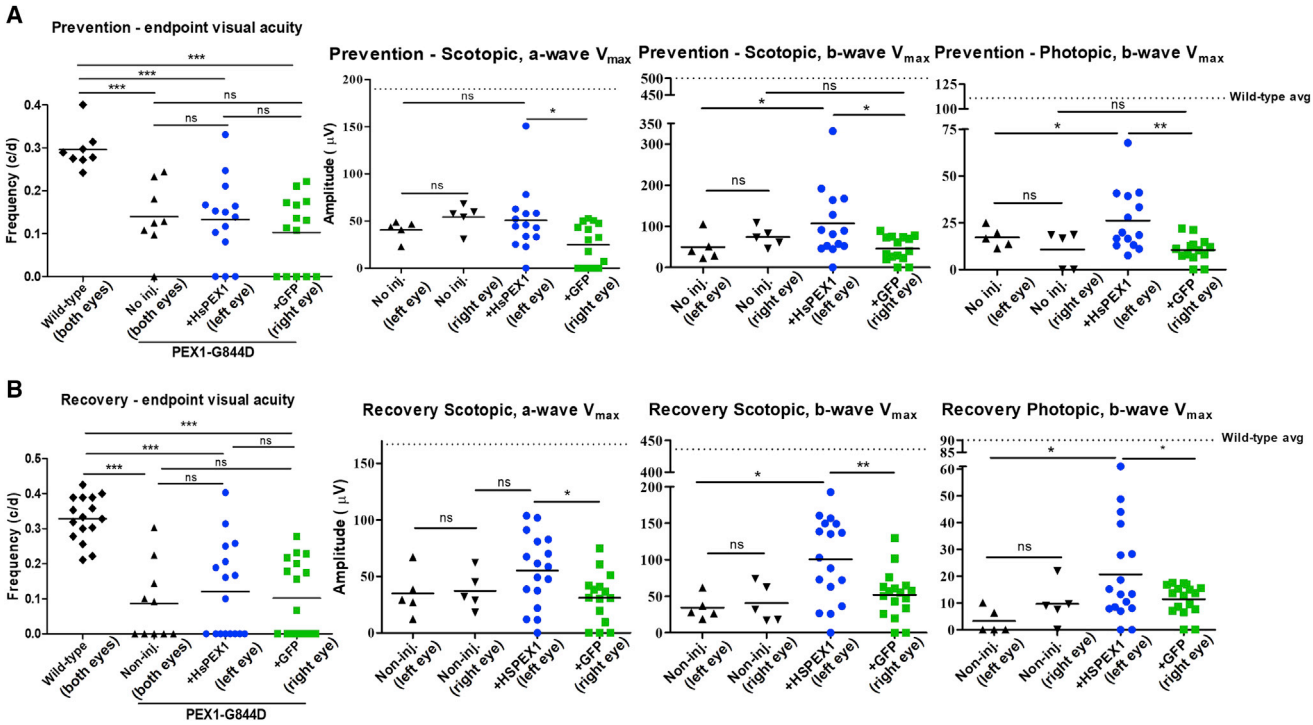

Figure 7. Prevention and recovery cohorts: endpoint ffERG and visual acuity measures at 32 weeks of age (6 or 7 months post-gene delivery for recovery or prevention cohorts, respectively)

(A) In the prevention cohort, the average maximal scotopic a-wave, scotopic b-wave, and photopic b-wave amplitude of the *HsPEX1*-injected left eyes was two-fold that of the GFP-injected right eyes. Average visual acuity trended higher in the left- versus right-injected eyes but was not statistically significant. (B) Similarly, in the recovery cohort, the average maximal scotopic a-wave, scotopic b-wave, and photopic b-wave amplitude of the *HsPEX1*-injected left eyes was two-fold that of *EGFP*-injected right eyes. Average visual acuity trended higher in left- versus right-injected eyes, but this was not statistically significant. In both cohorts, the retinal response of *EGFP*-injected eyes did not differ from that of either eye in non-injected mutant concurrent controls. As there was no difference between wild-type mice with or without subretinal injection, these values are thus grouped together. Upper dotted line represents wild-type average (n = 4–8). Scotopic ffERG response at highest stimulus interval (0.9 log cd.s.m^{-2}) is shown. Each point represents 1 mouse; Student's t test, *p < 0.05, **p < 0.01, ***p < 0.001, and ns, non-significant at p < 0.05. See Figure S4 for ERG waveforms.

photoreceptor dysfunction precedes RPE degeneration, evidenced by histological observations at 4 weeks of age (Figure S5), this does not preclude RPE degeneration contributing to photoreceptor decline. Although the higher enrichment of PEX1 in photoreceptor cells suggests a cell-autonomous function for PEX1 in photoreceptors, this does not rule out non-cell autonomous interactions with the RPE, which also contains peroxisomes and PEX1 protein. Techniques such as imaging MS to correlate the location and amount of vector expression with peroxisome recovery and functional outcome should be considered to address relevant questions in future.

Retinal C26:0 lyso-PCs only improved in the earlier-treated prevention cohort, perhaps due to decreased photoreceptor density at 9 compared to 5 weeks (see Figure S6), in that fewer "rescuable" cells remain in mice treated at 9 weeks. However, the extent to which VLCFA elevation contributes to retinopathy in PEX1-G844D mice and ZSD remains unclear. Elevated VLCFA is associated with retinal dysfunction in other peroxisome diseases, such as MFP2D,[44] but not in X-linked adrenoleukodystrophy, in which retinopathy is absent despite elevated VLCFA. Adult Refsum disease (which features retinopathy) is caused by accumulation of dietary phytanic acid, which is not elevated in PEX1-G844D fibroblasts, despite decreased phytanic acid oxidation (although phytanic acid was never measured in retina).[23] Finally, plasmalogens are not decreased in PEX1-G844D retinas, despite decreased circulating levels, and C27 bile acid intermediates were not detectable in our PEX1-G844D retinas, despite elevated circulating levels. Taken together, these observations suggest tissue-specific differences in peroxisome functions in this model, which warrants mechanistic studies of metabolic etiology.

Clinical implications

In the homozygous PEX1-G844D mouse retina, the murine PEX1-G844D mutant protein is detected at levels consistent with wild-type murine PEX1 protein levels in controls.[24] Thus, in our gene augmentation studies, the AAV-delivered HsPEX1 protein is likely competing with endogenous PEX1-G844D protein for inclusion in murine exportomer complexes. In contrast, HsPEX1-G843D protein amounts are reduced to 5%–15% of normal PEX1 amounts in patient fibroblasts (the only tissues studied), with PEX6 and PEX5 protein amounts also markedly diminished.[45–47] If PEX1-G843D protein levels are

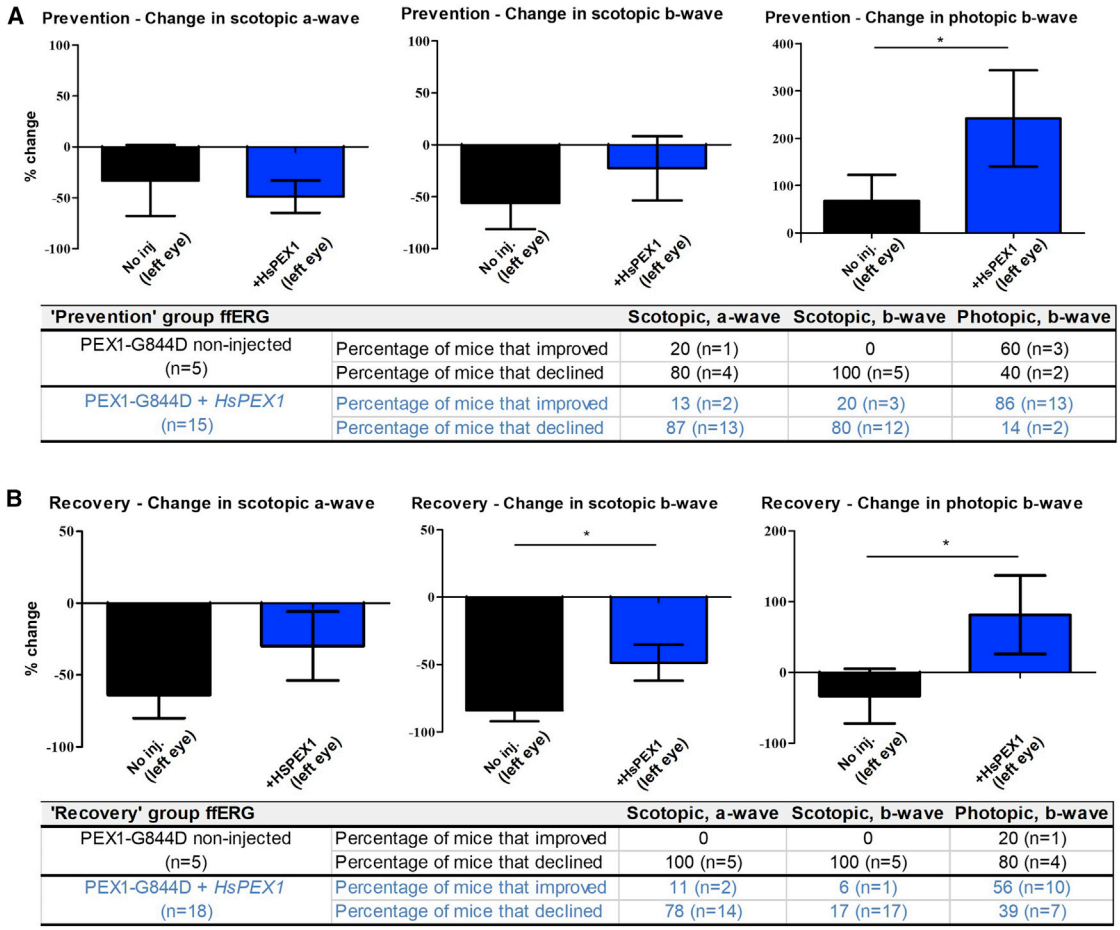

'Prevention' group ffERG		Scotopic, a-wave	Scotopic, b-wave	Photopic, b-wave
PEX1-G844D non-injected (n=5)	Percentage of mice that improved	20 (n=1)	0	60 (n=3)
	Percentage of mice that declined	80 (n=4)	100 (n=5)	40 (n=2)
PEX1-G844D + *HsPEX1* (n=15)	Percentage of mice that improved	13 (n=2)	20 (n=3)	86 (n=13)
	Percentage of mice that declined	87 (n=13)	80 (n=12)	14 (n=2)

'Recovery' group ffERG		Scotopic, a-wave	Scotopic, b-wave	Photopic, b-wave
PEX1-G844D non-injected (n=5)	Percentage of mice that improved	0	0	20 (n=1)
	Percentage of mice that declined	100 (n=5)	100 (n=5)	80 (n=4)
PEX1-G844D + *HsPEX1* (n=18)	Percentage of mice that improved	11 (n=2)	6 (n=1)	56 (n=10)
	Percentage of mice that declined	78 (n=14)	17 (n=17)	39 (n=7)

Figure 8. Subretinal gene delivery slows the decline in rod function and improves cone function

The percent change from baseline to endpoint ffERG was calculated for each mouse in the (A) prevention cohort and (B) recovery cohort and plotted for PEX1-G844D homozygous mice that received either no injection (black) or *HsPEX1* subretinal gene delivery (blue). Overall, the average decline in scotopic ffERG was less, and the photopic ffERG improved in *HsPEX1*-injected eyes compared to non-injected eyes in both cohorts. The number and proportion of mice for which ffERG improved or declined by at least 10% are represented in tables below plots and demonstrate an overall greater incidence of improvement in treated versus untreated mice. Mean ± SD is shown. Student's t test, *$p < 0.05$. See Figures S3 and S4 for baseline and endpoint ffERG waveforms.

also reduced in patient photoreceptor cells, then the transgene-encoded PEX1 protein would have a decided advantage for inclusion in exporter complexes. The difference in PEX1 stability is more likely species specific than tissue specific, as the observation holds true for all mouse tissue examined (fibroblasts, retina, liver, brain, kidney, lung, heart, and thymus). This may have positive implications for retinal gene augmentation therapy in ZSD patients, as competition against the endogenous mutant protein would be reduced.

Our proof-of-concept study represents the first application of gene augmentation therapy to treat a peroxisome biogenesis disorder and highlights the potential to retain and/or improve retinal function even after the onset of retinal degeneration in milder ZSD. Given that visual care is supportive only, gene augmentation therapy could benefit retinal functions in milder patients with a host of hypomorphic *PEX1* alleles. Although a multisystemic disorder, retinal therapies would benefit a large proportion of ZSD patients, improving communication, learning, autonomy, and overall quality of life.

MATERIALS AND METHODS

Proviral plasmids and AAV production

Human codon optimized *PEX1* sequence (synthesized by DNA2.0; ATUM, Newark, CA, USA) was amplified with Q5 DNA polymerase (New England Biolabs, Ipswich, MA, USA) to include a Kozak consensus sequence preceding the translational start site and a C-terminal HA epitope tag. This PCR product was digested with *NotI*-HF® and *ScaI*-HF® restriction enzymes (New England Biolabs, Ipswich, MA, USA) and cloned into an AAV proviral plasmid using the T4 DNA ligase (New England Biolabs, Ipswich, MA, USA). The completed proviral vector consisted of the CMV enhancer/promoter driving transgene expression and terminating with the bGH polyadenylation signal. The expression cassette was flanked by the canonical

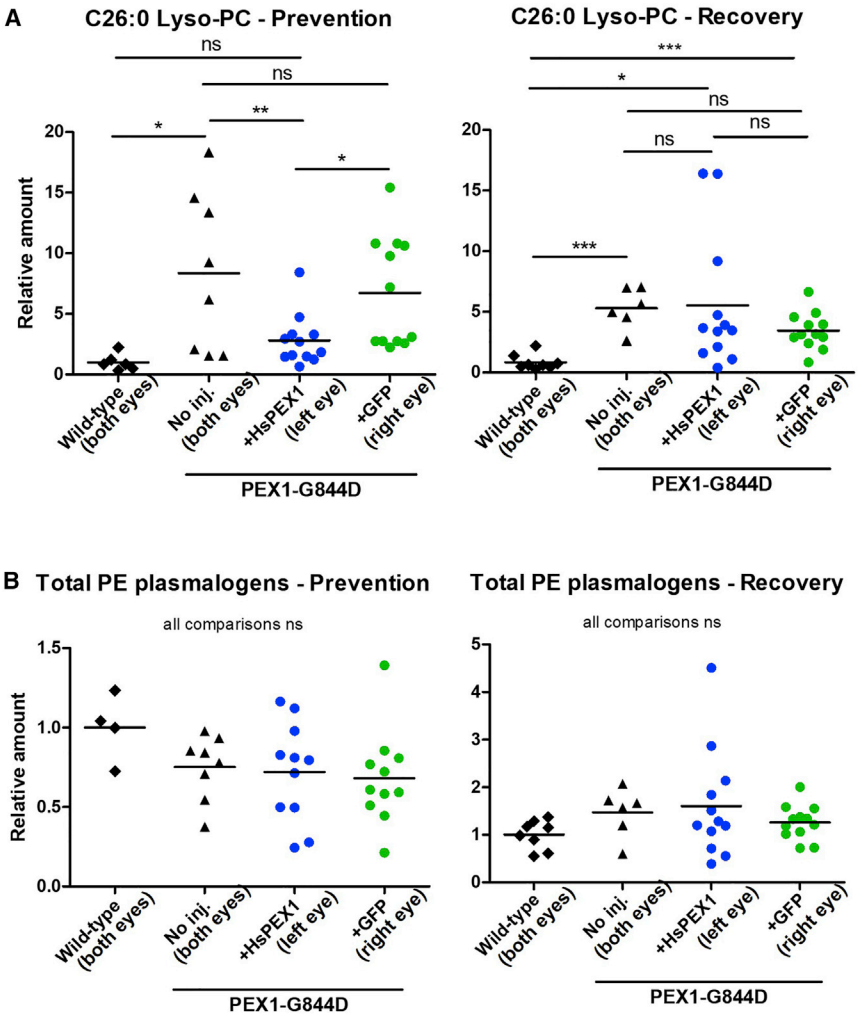

Figure 9. Improvement of peroxisome metabolites in retinas from prevention and recovery cohorts

Very long chain fatty acids (VLCFAs; measured as C26:0 lyso-PC) and phosphoethanolamine (PE) plasmalogens were measured by LC-MS/MS in mouse retinas at experimental endpoints. (A) Average C26:0 lyso-PC levels were increased 5- to 7-fold in untreated PEX1-G844D mice compared to wild-type littermate controls. In the prevention cohort, C26:0 lyso-PCs were significantly decreased in the *PEX1*-injected left eyes and no longer differed significantly from wild-type. This effect was not achieved in the recovery cohort. (B) PE plasmalogens amounts were not abnormal in this model and remained unchanged after gene delivery in both cohorts. Biochemical metabolite levels were originally calculated as nanomoles per milligram protein, and results are demonstrated by normalizing all values against the wild-type average for each experiment (set to "1"). Each point represents one whole retina; Student's two-tailed t test, $^{*}p < 0.05$, $^{**}p < 0.01$, $^{***}p < 0.001$, and ns, non-significant at $p < 0.05$.

AAV2 ITRs. AAV8 vectors (Center for Advanced Retinal and Ocular Therapeutics Research Vector Core, University of Pennsylvania, Philadelphia, PA, USA) were generated using previously described methods[48] by branched polyethylenimine (PEI) (23966; Polysciences, Warrington, PA, USA)-mediated triple transfection of HEK293 cells with a plasmid containing the transgene inserted between the ITRs of AAV2, the AAV helper plasmid encoding Rep2 and Cap for serotype variants, and the pHGTI-Adeno1 plasmid harboring helper adenoviral genes. The HEK293 cells express the helper E1A/E1b gene (CRL-157; American Type Culture Collection, Manassas, VA, USA). Vectors were purified using a discontinuous iodixanol gradient (Optiprep; Sigma-Aldrich, St. Louis, MO, USA). Encapsidated DNA was quantified by TaqMan RT-PCR, following denaturation of the AAV particles by proteinase K; titers were calculated as genome copies (gcs) per milliliter. Virus was stored at −80°C until use.

In vitro titer assay for individual AAV capsid variants

Capsid genes were cloned in an AAV packaging plasmid for vector production and used for small-scale vector preparations encoding firefly luciferase to obtain the titer. Physical particle titers were established by TaqMan qPCR. Subsequently, AAV2/8 bp variants were assayed for transduction at equal MOI onto HEK293 cells. For large-scale viral titer, the encapsidated DNA was quantified by TaqMan RT-PCR following denaturation of the AAV particles by proteinase K, and titers were calculated as gcs per milliliter.

Cell transduction and immunoblotting

AAV8.CMV.*HsPEX1.HA* or AAV8.CMV.EGFP was added to 84-31 cells (a modified HEK293 cell line) at a MOI of 10^5 or 5×10^5 (10 μL or 50 μL of 10^{10} vg/μL per 2×10^6 cells at time of viral expression). Cells were harvested after 48 h, lysed, and separated on a 4%–12% Bis-Tris gradient gel (Invitrogen, Waltham, MA, USA) and transferred to nitrocellulose membrane. Membranes were blocked in 5% milk and hybridized in 2% milk with 1:1,000 rabbit anti-HA tag (3724; Cell Signaling Technology, Danvers, MA, USA), 1:1,000 rat anti-GFP (04404-84; Cedarlane, Burlington, ON, Canada), and 1:15,000 rabbit anti-human β-tubulin (ab6046; Abcam, Cambridge, MA, USA), followed by appropriate horseradish peroxidase (HRP)-conjugated secondary antibody and visualized by enhanced chemiluminescence (ECL) using an Amersham 600 Imager. Mouse retina immunoblotting followed the same method, with the addition of 1:1,000 rabbit anti-HsPEX1 (13669-1-AP; Proteintech, Rosemont, IL, USA).

Peroxisome import after viral transduction

Human cells

HepG2 control and PEX1 null cells generated using CRSPR-Cas9-mediated gene editing to disrupt the gene were seeded onto coverslips

in 12-well plates and transduced with AAV8.CMV.*HsPEX1.HA* or AAV8.CMV.*EGFP* at an MOI of 10^5.

Mouse cells

p.Receiver-Lv219 (EX-T0228-Lv219; GeneCopoeia, Rockville, MD, USA) expressing *HsPEX1* cDNA (human transcript ID, GenBank: NM_000466.2) downstream of a CMV promoter (CMV-PEX1-IRES2-Puro) or *HsPEX1*-c.2097_2098insT (*HsPEX1* null allele generated by modifying the former construct by site-directed mutagenesis), pMD2.G, and psPAX2 (Addgene, Watertown, MA, USA) were packaged into lentivirus using HEK293T cells. Supernatant was filtered and concentrated with a Lenti-X Concentrator (631231; Clontech Laboratories, Mountain View, CA, USA) and applied to primary mouse wild-type and PEX1-G844D homozygous fibroblasts seeded in 12-well plates. After 2 rounds of transduction, positively transduced cells were selected with 0.25 μg/mL puromycin for 10 days and applied to coverslips for imaging.

IF

Cells were prepared for indirect IF as previously described,[29] mounted onto slides using ProLong Gold Antifade Reagent with DAPI (Invitrogen, Waltham, MA, USA), and visualized using a Leica DMI600 microscope with a DFC345FX camera and LASX software (Leica, Richmond Hill, ON, Canada). Primary antibodies used were 1:300 rabbit anti-PTS1 (generated and gifted by Dr. Steven Gould, Johns Hopkins University, Baltimore, MD, USA), 1:150 mouse anti-human ABCD3 (SAB4200181; Sigma-Aldrich, St. Louis, MO, USA), and 1:300 rabbit anti-HsPEX5 (generated and gifted by Dr. Gabriele Dodt, University of Tübingen, Germany). Secondary antibodies used were 1:400 Alexa Fluor 488 anti-rabbit (A21206; Invitrogen, Waltham, MA, USA) and 1:300 Alexa Fluor 594 anti-mouse (A11005; Invitrogen, Waltham, MA, USA).

Animal husbandry

PEX1-G844D mice were maintained on a mixed 129/SvEv and C57BL/6N Taconic background. Strain background was evaluated yearly by SNP genotyping (MaxBax; Charles River Laboratories, Cambridge, MA, USA) and showed a stable 70% 129/SvEv and 30% C57BL/6N Taconic. Colony founder mice used to breed experimental animals were negative for the *Rd8* mutation of the *Crb1* gene (genotyping performed as described by Mattapallil et al.[49]). Mice were housed at the Research Institute of the McGill University Health Centre (RI-MUHC) Glen site animal care facility with *ad libitum* access to food and water. All experiments were performed at the RI-MUHC Glen site, except for visual acuity measures, which were performed at the Pavillon Liliane-de-Stewart de l'Université de Montréal animal care facility. All experiments were approved by the RI-MUHC Animal Care Committee or the Université de Montréal Ethics Committee. Euthanasia was performed by CO_2 under isoflurane anesthesia (5% isoflurane in oxygen until loss of consciousness, immediately followed by CO_2 at maximum flow rate, 4 L/min). Both males and females were used for all experiments and wild-type and PEX1-G844D heterozygous mice used as littermate controls. There were no phenotypic differences based on sex or control genotype. Genotyping was performed as previously described.[24] At experimental endpoint, tail snips were collected and stored for future SNP genotyping to confirm strain background and absence of *Crb1* gene *Rd8* mutation.

Design of *in vivo* experiments

Experiments were done using 2 different age cohorts to test the effect of intervention at early and later disease stages. A validation cohort was included for the purpose of early confirmation of vector-mediated protein expression and to determine extent and localization of expression. To account for variability among individual mice, each injected mouse received therapeutic vector in the left eye and GFP vector in the right eye. OMR measures were only acquired at the experimental endpoint, since they were performed at a different animal care facility, and due to facility import restrictions, the mice could not be returned for subsequent ffERGs

Prevention cohort

Baseline ffERGs were at 4 weeks of age and injection at 5 weeks of age. Preliminary ffERGs were done on a subset of animals 5 months post-injection (25 weeks of age). Final ffERGs were done 7 months post-injection and visual acuity (OMR) 7.5 months post-injection (31−33 weeks of age), after which mice were sacrificed and both retinas used for LC-MS/MS analyses. Animal numbers at endpoints included 15 injected mutants, 4 non-injected mutants, 2 injected wild-type littermates, and 4 non-injected wild-type littermates.

Recovery cohort

Baseline ffERGs were at 8 weeks of age and injection at 9 weeks of age. Preliminary ffERGs were done on a subset of animals 4 months post-injection (25 weeks of age). Final ffERGs were done 6 months post-injection and OMR 6.5 months post-injection (31−33 weeks of age), after which mice were sacrificed and both retinas used for LC-MS/MS analyses. Animal numbers at endpoints included 18 injected mutants, 6 non-injected mutants, 4 injected wild-type littermates, and 4 non-injected wild-type littermates.

Validation cohort

There was no baseline ffERG; injection was at 5 or 9 weeks of age. A subset of mice (n = 4) were sacrificed 4 weeks post-injection to confirm HsPEX1.HA expression by IHC and immunoblot. ffERG was done on the remaining mice 8 weeks post-injection (13 or 17 weeks of age) and OMR at 11 weeks post-injection (16 or 20 weeks of age). Mice were sacrificed 12 weeks post-injection and both eyes processed for IHC. Animal numbers included 7 injected at 5 weeks of age and 6 injected at 9 weeks of age.

Vector delivery

Virus was diluted to 1.03×10^{10} vg/μL (AAV8.CMV.*HsPEX1.HA*) or 1.40×10^{10} vg/μL (AAV8.CMV.*EGFP*) in Pluronic F-127 buffer (Sigma-Aldrich, St. Louis, MO, USA). Mice received meloxicam oral analgesic in suspension and were anesthetized by intraperitoneal injection of 130 mg ketamine and 13 mg xylazine in sterile PBS per kilogram body weight. Proparacaine hydrochloride (Alcaine; Alcon, Mississauga, ON, Canada) was applied to the eye and pupils dilated

using tropicamide (Mydriacyl; Alcon, Mississauga, ON, Canada). Bilateral subretinal injections to deliver 1 μL virus dilution per eye were performed as previously described.[50] AAV8.CMV.*HsPEX1*.HA was delivered to the left eye, and AAV8.CMV.EGFP to the right. Tobramycin/dexamethasone ointment (Tobradex; Alcon, Fort Worth, TX, USA) was applied to eyes for 2 days following surgery. Injections were performed in the animal surgical suite of the RI-MUHC Glen animal facility under a dissecting microscope. Mice were observed for signs of discomfort or corneal injury.

Electrophysiology

Retinal function was assessed using ffERG as previously described.[24,51] Following a 12-h dark-adaptation period, mice were anesthetized (intraperitoneal injection of 130 mg ketamine and 13 mg xylazine in sterile PBS per kilogram body weight), and their pupils were dilated (1% Mydriacyl tropicamide [Alcaine; Alcon, Mississauga, ON, Canada]). All experimental procedures were performed in a dark room under red light illumination. Two types of recordings were performed to assess rod and cone function: scotopic or dark-adapted ffERG and photopic or light-adapted ffERG, respectively. Scotopic ffERGs were obtained from fully dark-adapted retinas in response to progressively brighter flashes of white light ranging in luminous intensity from -6.3 log cd.s.m^{-2} to -1.5 log cd.s.m^{-2} in 0.9 log-unit increments and from -1.5 log cd.s.m^{-2} to 0.9 log cd.s.m^{-2} in 0.3 log-unit increments (interstimulus interval: 10 s, flash duration 20 μs, average of 3–5 flashes depending on luminance). Photopic ffERGs were evoked to flashes of 0.9 log cd.s.m^{-2} (photopic background, 30 cdm^{-2}, interstimulus interval: 1 s, flash duration 20 μs, average of 20 flashes). In order to avoid any light-adaptation effect, the photopic recordings were obtained 20 min following the opening of the background light. Quantification of the amplitude of the a-wave and b-wave was performed as previously described.[52] Briefly, the amplitude of the a-wave was measured from baseline to the most negative trough, whereas the amplitude of the b-wave was measured from the trough of the a-wave to the most positive peak of the ffERG (scotopic ffERG) and from the baseline to the highest peak of the b-wave (photopic ffERG). ffERGs were performed at baseline and at 2, 4, 5, and 6–7 months post-gene delivery. Since our PEX1-G844D mice do not exhibit a different response pattern to increasing stimulus compared to control (i.e., the greater the stimulus, the greater the ffERG response), we chose only to show the ffERG response at the highest intensity in the figures.

Visual acuity using the virtual optomotor system

The spatial frequency threshold ("visual acuity") of the OMR of mice was determined using a virtual-reality optomotor system (Cerebral Mechanics, Lethbridge, AB, Canada) as previously described.[53] Briefly, freely moving mice were placed on an elevated platform and exposed to vertical sine-wave gratings rotating at 12°/s. The grating spatial frequencies increased from 0.01 to 0.5 cycles/degree in varying increments. When able to perceive the stimulus, the mouse normally stopped moving its body and began to track the grating with reflexive head movements in concert with the rotation. Spatial frequency of the grating at full contrast (100%) was gradually increased until the mice no longer exhibited a tracking behavior. The highest spatial frequency that could be followed (i.e., spatial frequency threshold) determined the visual acuity (in cycles per degree) for each eye. This technique yields independent measures of right- and left-eye acuity, as only motion in the temporal-to-nasal direction evokes a tracking response. Mice were tested within 3 h of their daylight hour onset.

Retinal IHC

For cryosections, eye cups from PBS-perfused mice were fixed 3 h in 10% formaldehyde; incubated in 10% (30 min on ice), 20% (1 h on ice), and 30% (4°C overnight) sucrose in 0.1 M PB; and then embedded and frozen in frozen-section compound (VWR, Mississauga, ON, Canada). 5 μm retinal cryo-sections were blocked (1% normal goat serum, 0.1% Triton X-100, 10% bovine serum albumin [BSA] in PBS) for 1 h, washed, incubated at 4°C overnight with primary antibody in incubation buffer (0.1% Triton X-100, 10% BSA in PBS), washed, incubated 90 min with secondary antibody, and washed. Coverslips were mounted using ProLong Gold antifade reagent with DAPI (Invitrogen, Burlington, CA, USA), and retinas were visualized using a Leica DMI600 microscope with a DFC345FX camera and LASX software (Leica, Richmond Hill, ON, Canada). The primary antibody used was 1:300 rabbit anti-HA tag (3724; Cell Signaling Technology, Danvers, MA, USA).

Retinal flatmount preparation and IF

Eyes were fixed in 4% formalin for 5 min at room temperature, a hole made in the cornea with a needle (27G), and fixed for additional 25 min. Eyes were sectioned at the limbus and anterior segments discarded. The posterior eye cups were collected and the neural retina detached from RPE/choroid/sclera. Neural retina flatmounts were incubated in 0.1% Triton X-100, 10% fetal bovine serum (FBS) in PBS (saturation buffer) for 45 min, and then overnight at 4°C with primary antibody or fluorescein peanut agglutinin (Vector Laboratories, Burlingame, CA, USA) in saturation buffer. RPE/choroid/sclera flatmounts were treated with PBS solution containing 0.1% Triton X-100 for 45 min and then incubated overnight at 4°C with primary antibody and/or TRITC phalloidin (ECM Biosciences, Versailles, KY, USA) for RPE cell-counter staining. IF was analyzed and images acquired using a Zeiss LSM780 laser-scanning confocal microscope. The primary antibodies used were rabbit anti-HA tag (3724; Cell Signaling Technology, Danvers, MA, USA) and rabbit anti-human cone arrestin (AB15282; Millipore, Burlington, MA, USA). Alexa Fluor 488- and 594-conjugated antibodies were used as secondaries (Invitrogen, Waltham, MA, USA).

Lipid analysis

Whole retinas from PBS-perfused mice were isolated, flash frozen, and stored at −80°C. For biochemical analysis of peroxisome metabolites by LC-MS/MS, retinas were homogenized in PBS using a mini pestle. 2:1 chloroform:methanol containing 0.05% butylhydroxytoluene (BHT) was added to 50 μg protein extract in a glass tube and incubated on an orbital shaker at room temperature for 2 h. Samples were centrifuged at 2,500 rpm for 10 min, and the supernatant was transferred to a clean glass tube. The supernatant was washed with 0.2 vol of purified water, mixed, and centrifuged at 2,000 rpm room

temperature for 5 min to separate the 2 phases. The upper phase was removed, and the lower phase was washed with Folch theoretical upper phase (3:48:47 chloroform:methanol:water). Samples were mixed and centrifuged at 2,000 rpm for 5 min, and the upper phase was removed. The lower phase was dried under nitrogen and then in a vacuum desiccator for 30 min. The dried lipid was dissolved in 3:2 hexane:isopropanol containing 10 ng each of internal standard, 16:0-D4 lyso-PAF (20.6 pmol), and D4-26:0-lysoPC (15.6 pmol). Samples were filtered by centrifugation (Spin-X Centrifuge Tube Filters; Corning Costar, Tewksbury, MA, USA) for 5 min. Filtrates were analyzed in Verex auto-sampler vials (Phenomenex, Torrance, CA, USA). A 2.1 × 50-mm, 1.7-μm chromatography column and a Waters (Milford, MA, USA) TQD (triple quadrupole) mass spectrometer interfaced with an Acquity UPLC (ultra-performance LC) were used in positive ion electrospray ionization (ESI)-MS/MS. The solvent systems were mobile phase A = 54.5% water/45% acetonitrile/0.5% formic acid; mobile phase B = 99.5% acetonitrile/0.5% formic acid with both solutions containing 2 mM ammonium formate. Injections of extracts dissolved in 3:2 isopropanol:hexane were made with initial solvent conditions of 85% mobile phase A/15% mobile phase B. The gradient employed was from 15% to 100% mobile phase B over a period of 2.5 min, held at 100% mobile phase B for 1.5 min before reconditioning the column back to 85% mobile phase A/15% mobile phase B for 1 min at a solvent rate of 0.7 mL/min. A column temperature of 35°C and an injection volume of 5 μL for plasmalogen and 10 μL for lysoPC were used for analysis. Ethanolamine plasmalogens were detected by multiple reaction monitoring (MRM) transitions representing fragmentation of [M + H] + species to *m/z* 311, 339, 361, 385, 389, and 390 for compounds with 16:1, 18:1, 20:4. 22:6, 22:4, and 18:0 at the sn-2 position, respectively. LysoPC species were detected by MRM transitions representing fragmentation of [M + H] + species to *m/z* 104. Reagents used were authentic plasmalogen standards; tetradeuterated internal standards 26:0-D4 lysoPC (Avanti Polar Lipids, Alabaster, AL, USA), 16:0-D4 lyso-PAF (Cayman Chemical, Ann Arbor, MI, USA), and high-performance LC (HPLC)-grade solvents (methanol, acetonitrile, chloroform, and water; Fisher Scientific, Waltham, MA, USA); formic acid (Honeywell Fluka); ammonium formate (Sigma-Aldrich, St. Louis, MO, USA); and PBS (Thermo Fisher Scientific, Waltham, MA, USA).

Statistical analysis

Cell-based experiments were replicated 3 times. For all quantitative measures, data were compared for statistical significance ($p < 0.05$) using an unpaired two-tailed Student's t test. Male and female mice were used in equal numbers, and no sex-related difference was observed.

SUPPLEMENTAL INFORMATION

Supplemental information can be found online at https://doi.org/10.1016/j.omtm.2021.09.002.

ACKNOWLEDGMENTS

We thank Jeannette Bennicelli (UPenn) for her contribution to previous vector design (not used in this study) and Ning Huang (USC) for *in vitro* validation. We thank the Global Foundation for Peroxisomal Disorders (GFPD) and the Wynne Mattefy Research Foundation (WMRF) for which their support made these experiments possible and vision opened the door to preventing blindness in this condition. We also acknowledge the ZSD patients and families whose courage inspires us. This work was funded by the GFPD and the WMRF to N.E.B. and J.G.H.; the Canadian Institutes of Health Research to N.E.B. (CIHR 12610), N.E.B. and P.L. (CIHR 34575), and J.-F.B. (CIHR 156029); the Fonds de Recherche du Québec - Santé to C.A. (FRQS Doctoral Training Award 32105); and the Center for Advanced Retinal and Ocular Therapeutics to J.B.

AUTHOR CONTRIBUTIONS

C.A. designed and conducted the experiments, performed statistical analyses, assembled the figures, and wrote the paper. A.P. analyzed ERG waveforms and aided with retinal dissections, retinal imaging, and figure preparation. J.Y.S. validated AAV expression, performed subretinal injections, and aided with experimental design. S.O. performed subretinal injections for early validation cohort, RPE and photoreceptor analyses on retinal flatmounts and prepared corresponding figures. B.S. cloned constructs used for lentiviral production. B.C. performed OMR measures with C.A. D.S.M. cloned AAV constructs. E.D.P. performed LC-MS/MS analyses. J.-F.B. provided use of the OptoMotry platform and is supervisor to B.C. J.B. designed and produced AAV vectors, consulted on experimental design, and is supervisor to J.Y.S. and D.S.M. J.G.H. designed experiments, provided engineered HepG2 cells and lentiviral constructs, and is supervisor to B.S. P.L. provided use of electrophysiology equipment and is supervisor to A.P. N.E.B. is the primary investigator and supervisor to C.A. All authors participated in manuscript editing.

DECLARATION OF INTERESTS

Subsequent to this work, AmorChem Therapeutics invested research funding for the continuation of this project, which continues under the direction of C.A., N.E.B., J.G.H., and J.B. Intellectual property filings were made for the use of *PEX1* gene therapy to treat ZSD.

REFERENCES

1. Argyriou, C., D'Agostino, M.D., and Braverman, N. (2016). Peroxisome biogenesis disorders. Transl. Sci. Rare Dis. *1*, 111–144.
2. Steinberg, S., Chen, L., Wei, L., Moser, A., Moser, H., Cutting, G., and Braverman, N. (2004). The PEX Gene Screen: molecular diagnosis of peroxisome biogenesis disorders in the Zellweger syndrome spectrum. Mol. Genet. Metab. *83*, 252–263.
3. Ebberink, M.S., Mooijer, P.A., Gootjes, J., Koster, J., Wanders, R.J., and Waterham, H.R. (2011). Genetic classification and mutational spectrum of more than 600 patients with a Zellweger syndrome spectrum disorder. Hum. Mutat. *32*, 59–69.
4. Falkenberg, K.D., Braverman, N.E., Moser, A.B., Steinberg, S.J., Klouwer, F.C.C., Schlüter, A., Ruiz, M., Pujol, A., Engvall, M., Naess, K., et al. (2017). Allelic Expression Imbalance Promoting a Mutant PEX6 Allele Causes Zellweger Spectrum Disorder. Am. J. Hum. Genet. *101*, 965–976.
5. Yik, W.Y., Steinberg, S.J., Moser, A.B., Moser, H.W., and Hacia, J.G. (2009). Identification of novel mutations and sequence variation in the Zellweger syndrome spectrum of peroxisome biogenesis disorders. Hum. Mutat. *30*, E467–E480.
6. Reuber, B.E., Germain-Lee, E., Collins, C.S., Morrell, J.C., Ameritunga, R., Moser, H.W., Valle, D., and Gould, S.J. (1997). Mutations in PEX1 are the most common cause of peroxisome biogenesis disorders. Nat. Genet. *17*, 445–448.

7. Collins, C.S., and Gould, S.J. (1999). Identification of a common PEX1 mutation in Zellweger syndrome. Hum. Mutat. *14*, 45–53.

8. Gärtner, J., Preuss, N., Brosius, U., and Biermanns, M. (1999). Mutations in PEX1 in peroxisome biogenesis disorders: G843D and a mild clinical phenotype. J. Inherit. Metab. Dis. *22*, 311–313.

9. Preuss, N., Brosius, U., Biermanns, M., Muntau, A.C., Conzelmann, E., and Gartner, J. (2002). PEX1 mutations in complementation group 1 of Zellweger spectrum patients correlate with severity of disease. Pediatr. Res. *51*, 706–714.

10. Nashiro, C., Kashiwagi, A., Matsuzaki, T., Tamura, S., and Fujiki, Y. (2011). Recruiting mechanism of the AAA peroxins, Pex1p and Pex6p, to Pex26p on the peroxisomal membrane. Traffic *12*, 774–788.

11. Miyata, N., and Fujiki, Y. (2005). Shuttling mechanism of peroxisome targeting signal type 1 receptor Pex5: ATP-independent import and ATP-dependent export. Mol. Cell. Biol. *25*, 10822–10832.

12. Birschmann, I., Rosenkranz, K., Erdmann, R., and Kunau, W.H. (2005). Structural and functional analysis of the interaction of the AAA-peroxins Pex1p and Pex6p. FEBS J. *272*, 47–58.

13. Schwerter, D.P., Grimm, I., Platta, H.W., and Erdmann, R. (2017). ATP-driven processes of peroxisomal matrix protein import. Biol. Chem. *398*, 607–624.

14. Kiel, J.A., Emmrich, K., Meyer, H.E., and Kunau, W.H. (2005). Ubiquitination of the peroxisomal targeting signal type 1 receptor, Pex5p, suggests the presence of a quality control mechanism during peroxisomal matrix protein import. J. Biol. Chem. *280*, 1921–1930.

15. Wanders, R.J., and Waterham, H.R. (2006). Biochemistry of mammalian peroxisomes revisited. Annu. Rev. Biochem. *75*, 295–332.

16. Govaerts, L., Monnens, L., Tegelaers, W., Trijbels, F., and van Raay-Selten, A. (1982). Cerebro-hepato-renal syndrome of Zellweger: clinical symptoms and relevant laboratory findings in 16 patients. Eur. J. Pediatr. *139*, 125–128.

17. Folz, S.J., and Trobe, J.D. (1991). The peroxisome and the eye. Surv. Ophthalmol. *35*, 353–368.

18. Das, Y., and Baes, M. (2019). Peroxisomal Disorders and Retinal Degeneration. Adv. Exp. Med. Biol. *1185*, 317–321.

19. Ratbi, I., Jaouad, I.C., Elorch, H., Al-Sheqaih, N., Elalloussi, M., Lyahyai, J., Berraho, A., Newman, W.G., and Sefiani, A. (2016). Severe early onset retinitis pigmentosa in a Moroccan patient with Heimler syndrome due to novel homozygous mutation of PEX1 gene. Eur. J. Med. Genet. *59*, 507–511.

20. Berendse, K., Engelen, M., Ferdinandusse, S., Majoie, C.B., Waterham, H.R., Vaz, F.M., Koelman, J.H., Barth, P.G., Wanders, R.J., and Poll-The, B.T. (2016). Zellweger spectrum disorders: clinical manifestations in patients surviving into adulthood. J. Inherit. Metab. Dis. *39*, 93–106.

21. Ratbi, I., Falkenberg, K.D., Sommen, M., Al-Sheqaih, N., Guaoua, S., Vandeweyer, G., Urquhart, J.E., Chandler, K.E., Williams, S.G., Roberts, N.A., et al. (2015). Heimler Syndrome Is Caused by Hypomorphic Mutations in the Peroxisome-Biogenesis Genes PEX1 and PEX6. Am. J. Hum. Genet. *97*, 535–545.

22. Majewski, J., Wang, Z., Lopez, I., Al Humaid, S., Ren, H., Racine, J., Bazinet, A., Mitchel, G., Braverman, N., and Koenekoop, R.K. (2011). A new ocular phenotype associated with an unexpected but known systemic disorder and mutation: novel use of genomic diagnostics and exome sequencing. J. Med. Genet. *48*, 593–596.

23. Hiebler, S., Masuda, T., Hacia, J.G., Moser, A.B., Faust, P.L., Liu, A., Chowdhury, N., Huang, N., Lauer, A., Bennett, J., et al. (2014). The Pex1-G844D mouse: a model for mild human Zellweger spectrum disorder. Mol. Genet. Metab. *111*, 522–532.

24. Argyriou, C., Polosa, A., Cecyre, B., Hsieh, M., Di Pietro, E., Cui, W., Bouchard, J.F., Lachapelle, P., and Braverman, N. (2019). A longitudinal study of retinopathy in the PEX1-Gly844Asp mouse model for mild Zellweger Spectrum Disorder. Exp. Eye Res. *186*, 107713.

25. US Food and Drug Administration (2017). FDA approves novel gene therapy to treat patients with a rare form of inherited vision loss, https://www.fda.gov/news-events/press-announcements/fda-approves-novel-gene-therapy-treat-patients-rare-form-inherited-vision-loss.

26. Trapani, I., and Auricchio, A. (2019). Has retinal gene therapy come of age? From bench to bedside and back to bench. Hum. Mol. Genet. *28* (R1), R108–R118.

27. Bennett, J. (2017). Taking Stock of Retinal Gene Therapy: Looking Back and Moving Forward. Mol. Ther. *25*, 1076–1094.

28. Ellis, B.L., Hirsch, M.L., Barker, J.C., Connelly, J.P., Steininger, R.J., 3rd, and Porteus, M.H. (2013). A survey of ex vivo/in vitro transduction efficiency of mammalian primary cells and cell lines with Nine natural adeno-associated virus (AAV1-9) and one engineered adeno-associated virus serotype. Virol. J. *10*, 74.

29. Slawecki, M.L., Dodt, G., Steinberg, S., Moser, A.B., Moser, H.W., and Gould, S.J. (1995). Identification of three distinct peroxisomal protein import defects in patients with peroxisome biogenesis disorders. J. Cell Sci. *108*, 1817–1829.

30. Maxwell, M.A., Nelson, P.V., Chin, S.J., Paton, B.C., Carey, W.F., and Crane, D.I. (1999). A common PEX1 frameshift mutation in patients with disorders of peroxisome biogenesis correlates with the severe Zellweger syndrome phenotype. Hum. Genet. *105*, 38–44.

31. Zaki, M.S., Heller, R., Thoenes, M., Nürnberg, G., Stern-Schneider, G., Nürnberg, P., Karnati, S., Swan, D., Fateen, E., Nagel-Wolfrum, K., et al. (2016). PEX6 is Expressed in Photoreceptor Cilia and Mutated in Deafblindness with Enamel Dysplasia and Microcephaly. Hum. Mutat. *37*, 170–174.

32. Smith, C.E., Poulter, J.A., Levin, A.V., Capasso, J.E., Price, S., Ben-Yosef, T., Sharony, R., Newman, W.G., Shore, R.C., Brookes, S.J., et al. (2016). Spectrum of PEX1 and PEX6 variants in Heimler syndrome. Eur. J. Hum. Genet. *24*, 1565–1571.

33. Braverman, N.E., Raymond, G.V., Rizzo, W.B., Moser, A.B., Wilkinson, M.E., Stone, E.M., Steinberg, S.J., Wangler, M.F., Rush, E.T., Hacia, J.G., and Bose, M. (2016). Peroxisome biogenesis disorders in the Zellweger spectrum: An overview of current diagnosis, clinical manifestations, and treatment guidelines. Mol. Genet. Metab. *117*, 313–321.

34. Heimler, A., Fox, J.E., Hershey, J.E., and Crespi, P. (1991). Sensorineural hearing loss, enamel hypoplasia, and nail abnormalities in sibs. Am. J. Med. Genet. *39*, 192–195.

35. Neuhaus, C., Eisenberger, T., Decker, C., Nagl, S., Blank, C., Pfister, M., Kennerknecht, I., Müller-Hofstede, C., Charbel Issa, P., Heller, R., et al. (2017). Next-generation sequencing reveals the mutational landscape of clinically diagnosed Usher syndrome: copy number variations, phenocopies, a predominant target for translational read-through, and *PEX26* mutated in Heimler syndrome. Mol. Genet. Genomic Med. *5*, 531–552.

36. Kemper, A.R., Brosco, J., Comeau, A.M., Green, N.S., Grosse, S.D., Jones, E., Kwon, J.M., Lam, W.K., Ojodu, J., Prosser, L.A., and Tanksley, S. (2017). Newborn screening for X-linked adrenoleukodystrophy: evidence summary and advisory committee recommendation. Genet. Med. *19*, 121–126.

37. Berendse, K., Boek, M., Gijbels, M., Van der Wel, N.N., Klouwer, F.C., van den Bergh-Weerman, M.A., Shinde, A.B., Ofman, R., Poll-The, B.T., Houten, S.M., et al. (2019). Liver disease predominates in a mouse model for mild human Zellweger spectrum disorder. Biochim. Biophys. Acta Mol. Basis Dis. *1865*, 2774–2787.

38. Demaret, T., Roumain, M., Ambroise, J., Evraerts, J., Ravau, J., Bouzin, C., Bearzatto, B., Gala, J.L., Stepman, H., Marie, S., et al. (2020). Longitudinal study of Pex1-G844D NMRI mouse model: A robust pre-clinical model for mild Zellweger spectrum disorder. Biochim. Biophys. Acta Mol. Basis Dis. *1866*, 165900.

39. Vandenberghe, L.H., Bell, P., Maguire, A.M., Xiao, R., Hopkins, T.B., Grant, R., Bennett, J., and Wilson, J.M. (2013). AAV9 targets cone photoreceptors in the nonhuman primate retina. PLoS ONE *8*, e53463.

40. Umino, Y., and Solessio, E. (2013). Loss of scotopic contrast sensitivity in the optomotor response of diabetic mice. Invest. Ophthalmol. Vis. Sci. *54*, 1536–1543.

41. Peirson, S.N., Brown, L.A., Pothecary, C.A., Benson, L.A., and Fisk, A.S. (2018). Light and the laboratory mouse. J. Neurosci. Methods *300*, 26–36.

42. Vandenberghe, L.H., Bell, P., Maguire, A.M., Cearley, C.N., Xiao, R., Calcedo, R., Wang, L., Castle, M.J., Maguire, A.C., Grant, R., et al. (2011). Dosage thresholds for AAV2 and AAV8 photoreceptor gene therapy in monkey. Sci. Transl. Med. *3*, 88ra54.

43. Das, Y., Roose, N., De Groef, L., Fransen, M., Moons, L., Van Veldhoven, P.P., and Baes, M. (2019). Differential distribution of peroxisomal proteins points to specific roles of peroxisomes in the murine retina. Mol. Cell. Biochem. *456*, 53–62.

44. Das, Y., Swinkels, D., Kocherlakota, S., Vinckier, S., Vaz, F.M., Wever, E., van Kampen, A.H.C., Jun, B., Do, K.V., Moons, L., et al. (2021). Peroxisomal Multifunctional Protein 2 Deficiency Perturbs Lipid Homeostasis in the Retina and Causes Visual Dysfunction in Mice. Front. Cell Dev. Biol. *9*, 632930.

45. Walter, C., Gootjes, J., Mooijer, P.A., Portsteffen, H., Klein, C., Waterham, H.R., Barth, P.G., Epplen, J.T., Kunau, W.H., Wanders, R.J., and Dodt, G. (2001). Disorders of peroxisome biogenesis due to mutations in PEX1: phenotypes and PEX1 protein levels. Am. J. Hum. Genet. *69*, 35–48.

46. Zhang, R., Chen, L., Jiralerspong, S., Snowden, A., Steinberg, S., and Braverman, N. (2010). Recovery of PEX1-Gly843Asp peroxisome dysfunction by small-molecule compounds. Proc. Natl. Acad. Sci. USA *107*, 5569–5574.

47. MacLean, G.E., Argyriou, C., Di Pietro, E., Sun, X., Birjandian, S., Saberian, P., Hacia, J.G., and Braverman, N.E. (2019). Zellweger spectrum disorder patient-derived fibroblasts with the PEX1-Gly843Asp allele recover peroxisome functions in response to flavonoids. J. Cell. Biochem. *120*, 3243–3258.

48. Bennicelli, J., Wright, J.F., Komaromy, A., Jacobs, J.B., Hauck, B., Zelenaia, O., Mingozzi, F., Hui, D., Chung, D., Rex, T.S., et al. (2008). Reversal of blindness in animal models of leber congenital amaurosis using optimized AAV2-mediated gene transfer. Mol. Ther. *16*, 458–465.

49. Mattapallil, M.J., Wawrousek, E.F., Chan, C., Zhao, H., Roychoudhury, J., Ferguson, T.A., et al. (2012). The Rd8 mutation of the Crb1 gene is present in vendor lines of C57BL/6N mice and embryonic stem cells, and confounds ocular induced mutant phenotypes. Invest. Ophthalmol. Vis. Sci. *53*, 2921–2927.

50. Song, J.Y., Aravand, P., Nikonov, S., Leo, L., Lyubarsky, A., Bennicelli, J.L., Pan, J., Wei, Z., Shpylchak, I., Herrera, P., et al. (2018). Amelioration of Neurosensory Structure and Function in Animal and Cellular Models of a Congenital Blindness. Mol. Ther. *26*, 1581–1593.

51. Polosa, A., Bessaklia, H., and Lachapelle, P. (2017). Light-Induced Retinopathy: Young Age Protects more than Ocular Pigmentation. Curr. Eye Res. *42*, 924–935.

52. Joly, S., Pernet, V., Dorfman, A.L., Chemtob, S., and Lachapelle, P. (2006). Light-induced retinopathy: comparing adult and juvenile rats. Invest. Ophthalmol. Vis. Sci. *47*, 3202–3212.

53. Prusky, G.T., Alam, N.M., Beekman, S., and Douglas, R.M. (2004). Rapid quantification of adult and developing mouse spatial vision using a virtual optomotor system. Invest. Ophthalmol. Vis. Sci. *45*, 4611–4616.